Phoremost Research in Bilkent University

E. Özbay, H. V. Demir, K. Güven, M. Gökkavas, İ. Bulu, K. Aydın, H. Çağlayan.

Nanotechnology Research Center and Faculty of Science, Bilkent University, 06800 Bilkent, Ankara, Turkey.

We review the research of our group on propagation and negative refraction of electromagnetic waves in metallodielectric photonic crystals (PCs), the design, fabrication, and testing of 100 GHz left-handed metamaterials, GaN based modulators for short optical wavelengths, and AlGaN based photodetectors that exhibit gain.

1. NEGATIVE REFRACTION OF ELECTROMAGNETIC WAVES BY METALLODIELECTRIC PHOTONIC CRYSTALS

An interesting phenomenon arising from the dispersion relation of photonic crystals is the so called negative refraction effect. In order to make use of the negative refraction effect in certain applications such as focusing of electromagnetic waves, one usually requires negative indices of refraction over a wide range of angles. This is still a major challenge for photonic crystal based structures, especially for metallic photonic crystals. Due to the very large dielectric constants of metals (especially in microwave region), the bands that exhibit negative refraction for metallic photonic crystals occur at higher frequencies when compared to the dielectric photonic crystals with the same lattice parameters. As a result, it is difficult to obtain negative refraction of electromagnetic waves for large incidence angles by using metallic photonic crystals. In this study, we showed that by adding a periodic dielectric perturbation to the metallic photonic crystal, one can increase the range of angles at which negative indices of refraction are observed.

The metallodielectric photonic crystal that we used in our experiments and calculations is a square lattice of metallic and dielectric rods. We considered TM-polarized EM waves in our calculations and experiments. We have shown that the first band of the metallodielectric photonic crystal is dramatically shifted towards lower frequencies when compared to the first band of the metallic photonic crystal. The lowering of the first band is important for achieving negative refraction for large incidence angles. The law of refraction for photonic crystals state that one needs to match the surface parallel wave vector components of the incident and transmitted electromagnetic waves. Conservation of the surface parallel component of the wave vector suggests that one way to increase the range of negatively refracted incidence angles is to reduce the radius of free-space equal-frequency contour. This can be achieved by choosing a lower frequency range at which one expects negative refraction. In addition, the shape and the size of the equal-frequency contours for the photonic crystal must be kept unchanged. Hence, lowering the bands without modifying the lattice parameters such as reducing the lattice constant increases the range of incidence angles that are negatively refracted.

We next show the equal frequency contours of the metallodielectric photonic crystal computed over the first Brillouin zone for the first band (Fig. 1). The group velocity of the transmitted electromagnetic waves can be calculated from the equal frequency contours. In addition, one can find the wave vector of the transmitted electromagnetic wave through the photonic crystal by matching the surface parallel components of the wave vectors of the incident electromagnetic waves and allowed Bloch modes. The surface of the photonic crystal is aligned such that the normal vector to the air–photonic crystal interface is along the Γ-M direction. The wave vectors of the transmitted waves are found from the conservation of the surface-parallel component of the wave vector. Figure 1 shows that for the plotted equal-frequency contours, the group velocity of the incident waves and the group velocity of the transmitted waves fall on opposite sides of the surface normal. Correspondingly, these waves are negatively refracted. For the plotted equal-frequency contours, the magnitude of the largest surface-parallel wave vector component in free space is smaller than the largest surface-parallel wave vector component in the photonic crystal. In addition, the group velocities in free space and the group velocities in the photonic crystal fall on different sides of the surface normal. As a result, for the plotted equal-frequency contours EM waves are negatively refracted for all incidence angles.

In order to demonstrate the negative refraction effect experimentally, we measured the electric field intensity along the surface of the photonic crystal at the output interface for various incidence angles. The experimental setup consists of transmitting horn antenna and receiving monopole antenna. When the electromagnetic waves are negatively refracted one expects to observe higher intensities in the negative side of the crystal. Wherever, for positive refraction one expects to observe higher intensities on the positive side of the metallodielectric photonic crystal. We found that between the frequencies of 9.25 and 10.3 GHz, waves emerge from the negative side of the PC for all incidence angles. Hence, between 9.25 and 10.3 GHz electromagnetic waves are negatively refracted by the PC. We further explored the negative refraction effect by measuring the electric field intensities on the output side of the photonic crystal over a 40x15 cm2 area. The measurements were carried out by using a precision X-Y stage with steps of 2.5 mm. The measurement results for an incidence angle of 25° are shown in Figs. 2 (a) and (b). Figure 2 (a) shows the electric field intensity for 9 GHz. Note that at 9 GHz the incident electromagnetic waves are positively refracted by the metallodielectric photonic crystal. On the other hand, Fig. 2 (b) shows the electric field

intensities for 9.7 GHz. Figure 2 (b) clearly demonstrates that the electromagnetic waves are negatively refracted at 9.7 GHz when they are incident by 25° on the metallodielectric photonic crystal.

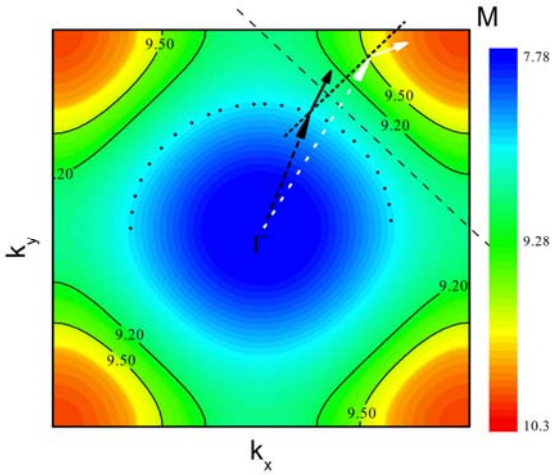

FIG. 1: Equal-frequency contours (solid curves) are shown for the metallodielectric photonic crystal. Crystal orientation is shown by the dashed line. Dotted circle represents the free-space equal-frequency contour at 9.5 GHz. Frequencies are shown in gigahertz. Long dashed arrow with black color represents the free-space wave vector whereas the short black arrow represents the free-space group velocity. Long dashed arrow with white color represents the wave vector of the refracted waves in the photonic crystal. Small white colored arrow indicates the direction of the group velocity inside photonic crystal.

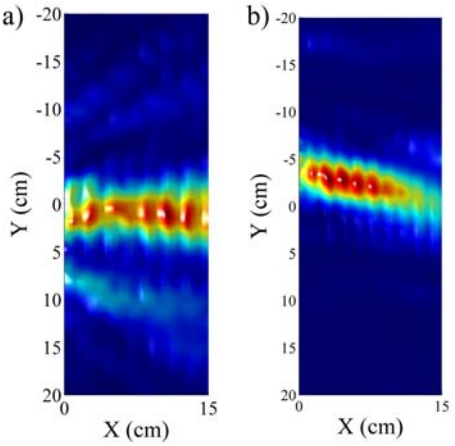

FIG.2: Electric field intensity at the exit of the metallodielectric photonic crystal.
a) Electric field intensity for 9 GHz (positive refraction). b) Electric field intensity for 9.7 GHz (negative refraction).
Incidence angle is 25 degrees.

2. A LEFT-HANDED METAMATERIAL OPERATING AT 100 GHZ

The idea of a left-handed (LH) material, first described by Veselago [1], was recently investigated experimentally [2, 3]. Such materials have large number of potential applications [4, 5]. First experimental realization of LH materials was achieved by separately constructing $\varepsilon < 0$ wire arrays [6], and $\mu < 0$ split-ring resonator (SRR) arrays [7], and then by combining them together forming a composite metamaterial (CMM) [2, 3, 8]. A SRR-only single layer operating at 100 THz [9] and a single layer CMM-type material operating at 2.5 THz [10] have been recently reported towards increased operating frequency. In this part, we report the smallest multilayer-CMM fabricated to date, which exhibits a LH transmission peak at 100 GHz and a negative index of refraction in this frequency range.

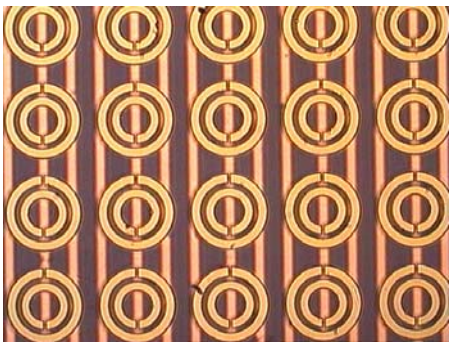

FIG. 3: Photomicrograph showing the mm-wave CMM sample.

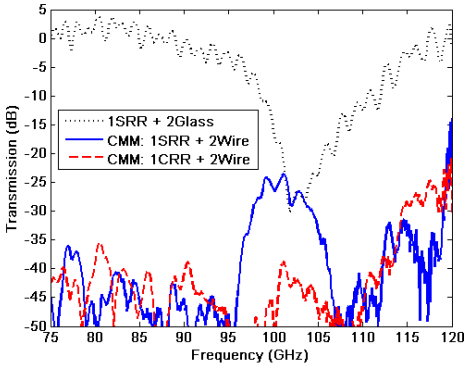

FIG. 4: Transmission spectra of CMM (SRR+wire) (solid), Closed-CMM (CRR+wire) (dashed) and SRR-only structures (dotted).

The metamaterial patterns for wire-, SRR-, and closed ring resonator (CRR)-arrays were printed on glass substrates by employing UV-photolithography followed by microfabrication. Figure 3 is a photomicrograph of one SRR-layer and one wire-layer stacked on top of each other. Figure 4 shows the transmission spectra of CMM structures incorporating SRRs, and CRRs, respectively, measured by a network analyzer. The CMM structure exhibits a pass band between 96 GHz to 107 GHz with a -25 dB maximum at 101 GHz. Note that this band matches the $\mu < 0$ stop band of SRRs. This is contrasted by the CMM incorporating CRR layers which remains opaque

throughout the frequency range. As a result, we conclude that the pass band of CMM indicates truly a left-handed behaviour. The left-handed nature of the peak was also proved by theoretical simulations.

3. GAN BASED QUANTUM MODULATORS FOR OPERATION AT SHORT OPTICAL WAVELENGTHS

Using wide-bandgap III-Nitrides, blue LEDs, blue lasers, and solar-blind detectors have been successfully demonstrated to date. III-N platform is, however, not limited only to these photonic devices and related applications and commercial interest. In our group, we aim to address this void in the device product line of III-N and expand their technological applications and commercial use important around the globe. As one such new III-Nitride nanophotonic device, we are developing optical quantum modulators that incorporate nano-scale quantum structures embedded in their p-i-n architecture for high-speed optical data coding from the visible (blue) to the ultraviolet (UV). These quantum modulators are expected to find applications in secure, point-to-point, optical communication in the UV (e.g., in space and underwater) and high-speed optical interconnects and clock injection directly into Si CMOS in the blue (e.g., at >10 Gbps). III-Nitride heterostructures exhibit large spontaneous and piezoelectric polarization fields, comparable to the levels of external electric fields typically used to observe the effect of quantum electroabsorption. This introduces a challenge for the design of the quantum electroabsorption structures. We use this extraordinary material property as an opportunity to design a new type of quantum electroabsorption structures, which we call "quantum zigzags" as shown in Fig. 5; the quantum zigzags rely on the alternating high polarization fields in the adjacent layers of the heterostructure. As shown in Fig. 6, the optical transmission spectrum measured from this quantum zigzag shows sharp absorption bandedge, which is a good sign for good electroabsorption behavior.

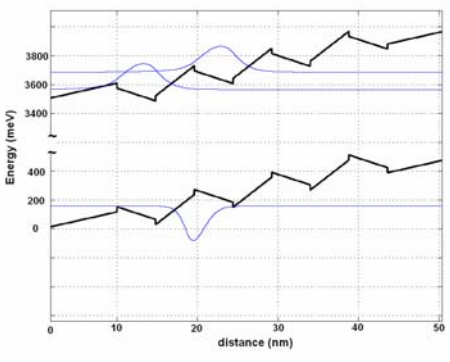

FIG. 5: Our quantum zigzag structure

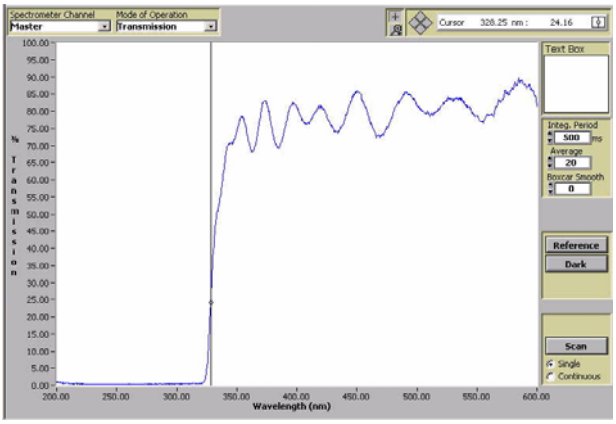

FIG. 6: Experimental optical transmission spectrum of the grown quantum zigzag structure with a sharp absorption band edge at ~326 nm.

4. SOLAR BLIND $AL_XGA_{1-X}N$ BASED AVALANCHE PHOTODIODES

Although a variety of high performance AlGaN photodetectors were reported, only very few GaN based avalanche photodiodes (APDs) were reported in the literature [11,12,13,14,15,16], and none reporting AlGaN based APDs. The high defect densities result in premature breakdown before the electric field can reach the bulk avalanche breakdown level, which is a major problem for the AlGaN/GaN APDs. In this part, we report the epitaxial growth, fabrication and characterization of AlGaN based APDs operating in the solar-blind spectral region.

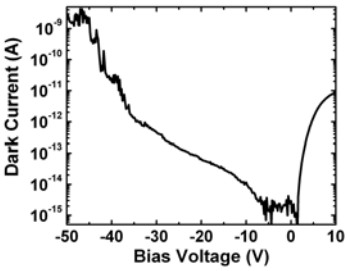

FIG. 7: Dark current of a 60 μm diameter photodetector.

The epitaxial structure of the front-illumination Schottky detector wafer was designed to achieve true-solar blindness, very low dark current, high solar rejection, and high breakdown. The AlxGa1-xN /GaN epitaxial layers of our heterojunction Schottky photodiode wafer were grown on a 2 in. single-side polished (0001) sapphire substrate using the Aixtron 200/4 RF-S MOCVD system located at Bilkent University Nanotechnology Research Center. The samples were fabricated by using a five-step microwave-compatible fabrication process in a class-100 clean room environment. The exact layer structure and fabrication sequence can be found in a recent report [17].

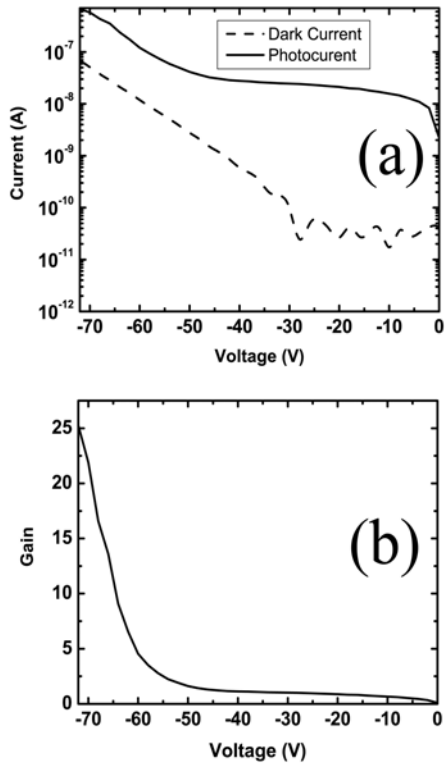

FIG. 8: (a) Dark current and photocurrent measurement of a 100 micron diameter photodetector (b) Corresponding avalanche gain of the same device.

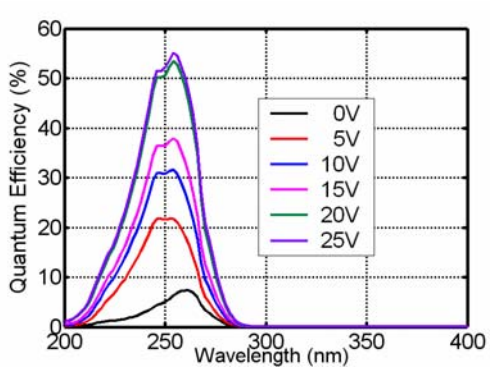

FIG. 9: Quantum efficiency measurements of a 100 μm diameter photodetector

The resulting devices had breakdown voltages higher than 50V. To obtain better isolation, we etched down to the sapphire substrate, which enabled us to obtain lower leakage current than previous fabrications. Figure 7 shows the dark current of a 60 μm diameter device. Dark current density at a 5 V reverse bias was 5.3x10-11 A/cm2. Up to 10V, the dark current was less than 10fA. At 50V bias, the device had a dark current of approximately 3 nA. The low dark current values proved the high growth quality of AlGaN wafer with low dislocation densities.

Figure 8(a) shows the current-voltage characteristics of a device with a 100 μm diameter. The device showed almost unity-gain behavior for voltages between 10 and 50 V, and the photocurrent was approximately 10 nA. After 50 volts, avalanche gain has been observed from the device. As shown in Figure 8(b), the maximum reproducible avalanche gain was 25 at 72V reverse bias.

Figure 9 shows the quantum efficiency measurements of a 100 μm diameter device for different bias voltages. Under a 25 V reverse bias voltage, the device had a maximum quantum efficiency of 55% at 254 nm. The cut-off wavelength was ~270 nm for all measurements.

[1] V. G. Veselago, Sov. Phys. Usp. **10**, 504 (1968).
[2] D.R. Smith, W.J. Padilla, D.C. Vier, S.C. Nemat-Nasser, and S.Schultz, Phys. Rev. Lett. **84**, 4184 (2000).
[3] R.A. Shelby, D.R. Smith, S.C. Nemat-Nasser, and S.Schultz, Apl. Phys. Lett. **78**, 480 (2001).
[4] N. Engheta, R.W. Ziolkowski, IEEE Tran. Microw. Theory Tech. **53**, 1535 (2005).
[5] J.B. Pendry, Phys. Rev. Lett. **85**, 3966 (2000).
[6] J.B. Pendry, A.J. Holden, W.J. Stewart, and I. Youngs, Phys. Rev. Lett. **76**, 4773 (1996).
[7] J.B. Pendry, A.J. Holden, D.J. Robbins, and W.J. Stewart, IEEE Trans. Microwave Theory Tech. **47,** 2075 (1999).
[8] K. Aydin, K. Guven, M. Kafesaki, L. Zhang, C. M. Soukoulis, and E. Ozbay, Opt. Lett. **29**, 2623 (2004).
[9] S. Linden, C. Enkrich, M. Wegener, J. Zhou, T. Koschny, and C. M. Soukoulis, Science **306**, 1351 (2004).
[10] H.O. Moser, B.D.F. Casse, O. Wilhelmi, and B.T. Saw, Phys. Rev. Lett. **94**, 063901 (2005).
[11] K. A. McIntosh, R. J. Molnar, L. J. Mahoney, A. Lightfoot, M. W. Geis, K. M. Molvar, I. Melngailis, R. L. Aggarwal, W. D. Goodhue, S. S. Choi, D.L. Spears, and S. Verghese, Appl. Phys. Lett. **75**, 3485 (1999).
[12] J. C. Carrano, D. J. H. Lambert, C. J. Eiting, C. J. Collins, T. Li, S. Wang, B. Yang, A. L. Beck, R. D. Dupuis, and J. C. Campbell, Appl. Phys. Lett. **76**, 924 (2000).
[13] A. Osinsky, M. S. Shur, R. Gaska, and, Q. Chen, Electron. Lett. **34**, 691 (1998).
[14] S. Verghese, K. A. McIntosh, R. J. Molnar, L. J. Mahoney, R. L. Aggarwal, M. W. Geis, K. M. Molvar, E. K. Duerr, I. Melngailis, IEEE Electron. Dev. Lett. **48**, 502 (2001).
[15] K. A. McIntosh, R. J. Molnar, L. J. Mahoney, K. M. Molvar, N. Efremov and S. Verghese, Appl. Phys. Lett. **76**, 3938 (2000).
[16] B. Yang, T. Li, K. Heng, C. Collins, S. Wang, J. C. Carrano, R. D. Dupuis, J. C. Campbell, M. J. Schurman and I. T. Ferguson, IEEE J. Quantum Electron. **36**, 1389 (2000).
[17] T.Tut, S. Bütün, B. Bütün, M. Gökkavas, H. Yu, and E. Özbay, Appl. Phys. Lett. **87**, 223502 (2005).